Radiology

Pulmonary Perfusion and Xenon Gas Exchange in Rats: MR Imaging with Intravenous Injection of Hyperpolarized ^{129}Xe[1]

Bastiaan Driehuys, PhD
Harald E. Möller, PhD
Zackary I. Cleveland, PhD
James Pollaro, MS
Laurence W. Hedlund, PhD

Purpose: To develop and demonstrate a method for regional evaluation of pulmonary perfusion and gas exchange based on intravenous injection of hyperpolarized xenon 129 (^{129}Xe) and subsequent magnetic resonance (MR) imaging of the gas-phase ^{129}Xe emerging in the alveolar airspaces.

Materials and Methods: Five Fischer 344 rats that weighed 200–425 g were prepared for imaging according to an institutional animal care and use committee–approved protocol. Rats were ventilated, and a 3-F catheter was placed in the jugular (n = 1) or a 24-gauge catheter in the tail ($n = 4$) vein. Imaging and spectroscopy of gas-phase ^{129}Xe were performed after injecting 5 mL of half-normal saline saturated with ^{129}Xe hyperpolarized to 12%. Corresponding ventilation images were obtained during conventional inhalation delivery of hyperpolarized ^{129}Xe.

Results: Injections of ^{129}Xe-saturated saline were well tolerated and produced a strong gas-phase ^{129}Xe signal in the airspaces that resulted from ^{129}Xe transport through the pulmonary circulation and diffusion across the blood-gas barrier. After a single injection, the emerging ^{129}Xe gas could be detected separately from ^{129}Xe remaining in the blood and was imaged with an in-plane resolution of 1×1 mm and a signal-to-noise ratio of 25. Images in one rat revealed a matched ventilation-perfusion deficit, while images in another rat showed that xenon gas exchange was temporarily impaired after saline overload, with recovery of function 1 hour later.

Conclusion: MR imaging of gas-phase ^{129}Xe emerging in the pulmonary airspaces after intravenous injection has the potential to become a sensitive and minimally invasive new tool for regional evaluation of pulmonary perfusion and gas exchange.

Supplemental material: *http://radiology.rsnajnls.org/cgi/content/full/2522081550/DC1*

[1] From the Center for In Vivo Microscopy, Duke University Medical Center, Box 3302, Durham, NC 27710 (B.D., Z.I.C., J.P., L.W.H.); Max Planck Institute for Human Cognitive and Brain Sciences, Leipzig, Germany (H.E.M.); and Department of Radiology, University Hospital Münster, Münster, Germany (H.E.M.). Received September 5, 2008; revision requested October 15; revision received December 16; accepted December 23; final version accepted January 15, 2009. Supported by the Gas Enabled Medical Innovations Fund 2005. **Address correspondence to** B.D. (e-mail: *Bastiaan.driehuys@duke.edu*).

The ability to assess ventilation, perfusion, and gas exchange is important for the management and study of pulmonary disease. These are currently measured by using pulmonary function testing, which evaluates the lung as a whole. However, it has been increasingly recognized that pulmonary function testing has limited sensitivity (1) because pulmonary disease is often heterogeneous and the considerable compensatory mechanisms of the lungs can obscure the presence of subtle regional disease when performing global measurements. Thus, it is important to develop methods that help evaluate lung function regionally. A growing need also exists for imaging in small animals to speed the development of novel therapies for pulmonary disease (2). Thus, pulmonary medicine would benefit from an integrated method for noninvasive regional mapping of all aspects of pulmonary function that can be applied from mouse to human (3).

Although ventilation and perfusion can be measured by using nuclear imaging methods (4,5) or, potentially, by using computed tomography (CT) (6–8), these methods deliver ionizing radiation that limits their use in longitudinal protocols. Furthermore, imaging of ventilation is now superbly performed with hyperpolarized gas magnetic resonance (MR) imaging by using the isotopes helium 3 (^{3}He) and xenon 129 (^{129}Xe) (9). Hence, it is desirable to extend this technology to include imaging perfusion and gas exchange, thereby making hyperpolarized gas MR imaging the spatially resolved, noninvasive analog of pulmonary function testing.

Advances in Knowledge

- A fundamentally new, minimally invasive imaging method to help visualize pulmonary perfusion and xenon gas exchange was introduced.
- A simple quantitative framework for understanding hyperpolarized ^{129}Xe magnetization dynamics in the pulmonary system as a means of optimizing image signal-to-noise ratio was presented.

Although considerable efforts have been applied to extract perfusion and gas exchange information from ^{3}He MR imaging results (10,11), the insolubility of ^{3}He in blood restricts it to being delivered by the airways. Pulmonary function can, in principle, be assessed more comprehensively by airway delivery of ^{129}Xe (12) because ^{129}Xe is soluble in blood and tissues, where it also exhibits readily discernible frequency shifts and retains longitudinal relaxation times of several seconds (13). These properties have been exploited to image pulmonary xenon gas exchange indirectly (14–16) and, more recently, by directly imaging the ^{129}Xe uptake in blood (17).

In contrast to airway delivery, we show a fundamentally new approach to delivering hyperpolarized ^{129}Xe—from the vascular side of the lungs (18). The subsequent emergence of ^{129}Xe in the airspaces is driven by both pulmonary perfusion and the exchange of xenon from the vasculature to the alveolar spaces. Although xenon differs from O_2 and CO_2 in physical and chemical properties, including solubility, diffusivity, and hemoglobin binding affinity, it traverses the same physical path as these metabolically important molecules during pulmonary gas exchange. Hence, xenon serves as a powerful probe of the gas exchange capacity of the pulmonary system. This process is outlined in Figure 1, which depicts hyperpolarized ^{129}Xe being mixed into saline and the saturated saline being injected intravenously in rats. Hyperpolarized ^{129}Xe, after injection, passes through the capillary beds of the lung and diffuses into the airspaces, where it can be selectively excited and imaged because gaseous ^{129}Xe resonates at a substantially different frequency than ^{129}Xe remaining in saline, blood, or tissues.

Materials and Methods

One author (B.D.) is a coinventor on the original patents covering hyperpolarized gas MR imaging and receives a small annual royalty for this.

Animal Preparation

Five Fischer 344 rats (Charles River Laboratories, Raleigh, NC) that weighed 200–425 g were prepared for imaging according to a protocol approved by our institutional animal care and use committee at Duke University Medical Center. Animals were first anesthetized with intraperitoneal injection of 65 mg sodium pentobarbital (Nembutal; Ovation Pharmaceuticals, Deerfield, Ill) per kilogram of body weight and 1 mg/kg butorphanol tartrate (Torbugesic; Fort Dodge Animal Health, Fort Dodge, Iowa), and anesthesia was maintained thereafter with periodic 20-mg/kg injections of sodium pentobarbital by using an intraperitoneal catheter. For ^{129}Xe-saline injection, a 3-F catheter (CC-3P; Access Technologies, Skokie, Ill) was placed in the right jugular vein (one rat) or a 24-gauge catheter (Autoguard-Winged; BD Medical Systems, Sandy, Utah) was placed in the tail vein (four rats). Rats were intubated with a 16-gauge catheter (Abbocath-T; Hospira Venisystems, Lake Forest, Ill) and were ventilated with a hyperpolarized gas–compatible constant-volume ventilator (19) at 60 breaths per minute with a tidal volume of 1 mL/100 g and a gas mixture of 25% O_2 and 75% N_2. The breathing gas could be switched by computer to replace the N_2 with hyperpolarized ^{129}Xe at an identical tidal volume for ventilation imaging. Each breath lasted 1 second and comprised a 240-msec inhalation, a 200-msec breath hold, and a 560-msec passive exhalation period. The animal was in the supine position in the imaging coil and

Published online before print
10.1148/radiol.2522081550

Radiology 2009; 252:386–393

Author contributions:
Guarantors of integrity of entire study, B.D., H.E.M., L.W.H.; study concepts/study design or data acquisition or data analysis/interpretation, all authors; manuscript drafting or manuscript revision for important intellectual content, all authors; manuscript final version approval, all authors; literature research, B.D., H.E.M., Z.I.C.; experimental studies, all authors; statistical analysis, H.E.M.; and manuscript editing, all authors

Funding:
This work was supported by a National Heart, Lung, and Blood Institute grant (5R21HL87094).

See Materials and Methods for pertinent disclosures.

See Science to Practice in this issue.

was inserted into the magnet, where its body temperature was continuously monitored with a rectal-temperature thermistor probe and was maintained at 37°C by warm air flowing through the magnet bore. The heart rate was monitored by using electrocardiographic electrodes taped to the foot pads.

Xenon 129 Polarization

Xenon, enriched to 83% ^{129}Xe (Spectra Gases, Alpha, NJ), was polarized with spin-exchange optical pumping (13) by using a prototype commercial polarizer (model 9800, Magnetic Imaging Technologies, Durham, NC). This system employs a continuous flow of dilute 1% xenon in 89% helium and 10% N_2 through an optical pumping cell containing rubidium where ^{129}Xe becomes polarized. After the mixture exits the optical cell, hyperpolarized ^{129}Xe is cryogenically extracted from the other buffer gases until a sufficient quantity is available for thawing and delivery (20). Hyperpolarized ^{129}Xe was produced for either injection or ventilation imaging in batches of 175 mL at polarizations of approximately 12% that took 20 minutes to accumulate.

MR Imaging Hardware

Images and spectra were acquired with a 2.0-T horizontal 30-cm clear bore magnet (Oxford Instruments, Oxford, England) with shielded gradients (180 mT/m) controlled by a console (EXCITE, version 12.0; GE Healthcare, Milwaukee, Wis). The imager was interfaced to the 23.66-MHz linear birdcage coil (8 cm long, 7 cm in diameter) by using an integrated transmit-receive switch with a 31-dB gain preamplifier (Nova Medical, Wilmington, Mass). The imager was operated at 23.66 MHz instead of its intrinsic 63.86-MHz frequency by using an up-down converter (Cummings Electronics Labs, North Andover, Mass).

Xenon 129 Dissolution and Injection

Hyperpolarized ^{129}Xe was dispensed from the polarizer into a 100-mL Pyrex shaker (21) containing 30–40 mL of half-normal saline (0.45% weight per volume NaCl) that had been degassed by evacuation with a rotary vane vacuum pump (Pfeiffer Vacuum, Nashua, NH). (Half-normal saline was selected because it clears more rapidly from the intravascular compartments than normal saline [22].) The hyperpolarized ^{129}Xe in the gas phase above the solution had a relaxation time of 700 seconds ± 160 (standard deviation), which provided a reasonable time to bring the shaker containing saline and hyperpolarized ^{129}Xe to the approximately 0.2-T fringe field of the MR imaging magnet, where it was shaken vigorously by hand for 20 seconds to dissolve the ^{129}Xe gas. Xenon 129 dissolved in the half-normal saline had a longitudinal relaxation time of 120 seconds ± 3 at 2 T, which was longer than the 66 seconds previously reported in normal saline at 9.4 T (23). This longer T1, presumably owing to reduced ion content, permitted a reasonable time for injection. A 5-mL volume of ^{129}Xe-saturated saline was withdrawn from the shaker into a 5-mL plastic syringe and was injected over a period of approximately 15 seconds through a 15-cm-long polyethylene catheter extension running into the MR imaging bore and connected to the venous catheter (Fig 1). The ^{129}Xe injection pathway consisted entirely of nonmetallic components, because materials such as stainless steel can rapidly depolarize hyperpolarized gases (24). The injection pathway had an estimated dead volume of less than 250 μL.

Xenon 129 MR Spectroscopy

Preimaging activities such as setting frequency, transmit gain, and shim were performed by first ventilating the rats with a 1% hyperpolarized ^{129}Xe mixture flowing directly and continuously from the polarizer (25). Specifically, the transmit gain was calibrated

Figure 1

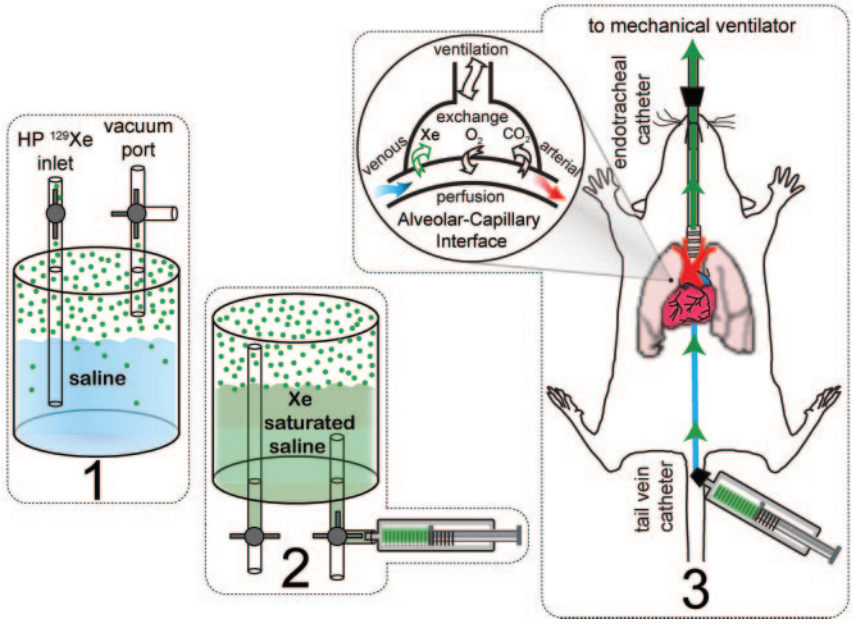

Figure 1: Dissolution of hyperpolarized *(HP)* ^{129}Xe into saline, injection of the xenon *(Xe)*-saturated solution, and excretion of hyperpolarized ^{129}Xe into the alveoli. *1,* Saline is degassed by evacuation, and gas-phase hyperpolarized ^{129}Xe is then introduced to the container. *2,* The container is manually shaken for 20 seconds to dissolve the hyperpolarized ^{129}Xe into the saline, and the saturated fluid is then withdrawn into an attached syringe. *3,* Saline is injected into venous blood, where it is transported to the lungs and excreted from the capillaries into the alveolar space. Hyperpolarized ^{129}Xe in the pulmonary airspaces has a substantially different resonance frequency than dissolved ^{129}Xe, which enables the gas phase to be selectively detected and imaged.

by increasing the applied radiofrequency power until a 180° pulse was obtained.

Several spectroscopy experiments were then performed during ^{129}Xe-saline injection to interrogate the ^{129}Xe signal dynamics in the lung and to optimize the acquisition parameters for imaging. Spectra were acquired without gating starting simultaneously with the ^{129}Xe-saline injection and by using a repetition time of either 125 or 250 msec. The injection lasted 15–20 seconds, while acquisition continued for 30 seconds (120–240 spectra) to fully capture the signal buildup and decay. Initial spectroscopy experiments were designed to probe the signal dynamics of the gaseous ^{129}Xe (0 ppm) and to probe those of ^{129}Xe dissolved in saline (195 ppm, +4615 Hz) and blood (215 ppm, +5088 Hz). These resonances were simultaneously excited by using a broadband hard pulse (132-μsec duration, approximately 7.6-kHz bandwidth, approximately 10° flip angle) centered at 102 ppm between the dissolved and airspace ^{129}Xe resonances. In our subsequent experiments, also performed without gating, only the airspace ^{129}Xe signal was probed by using a narrowband selective radiofrequency pulse (1.2 msec long, three-lobe sinc, 3.3-kHz bandwidth) centered at the 0-ppm airspace resonance. This pulse, when applied at the dissolved-phase resonance, produced no observable gas-phase signal and thus could be assumed to leave the dissolved ^{129}Xe magnetization source unaffected when applied at the gas-phase resonance. In these experiments, 10°, 20°, 30°, 45°, 60°, and 90° pulses were used to determine the optimal flip angle.

Xenon 129 MR Imaging Sequences

Images after vascular injection of the ^{129}Xe-saline mixture were acquired with the transmit frequency centered on the gas-phase ^{129}Xe resonance and with a pulse bandwidth of 3.3 kHz (see Xenon 129 MR Spectroscopy section) so that only gas-phase ^{129}Xe was excited. The airspace ^{129}Xe signal emerging after injection was spatially encoded by using a two-dimensional gradient-recalled echo sequence employing a sequential phase-encoding order without section selection (repetition time msec/echo time msec, 250/6.9; bandwidth, 4 kHz; matrix, 64 × 64; and field of view, 6.4 cm to yield an image resolution of 1 × 1 mm). Image acquisition was initiated approximately 5 seconds after the start of ^{129}Xe-saline injection to allow sufficient time for ^{129}Xe to reach the lungs. The acquisition had a flip angle of 15° that was determined to be optimal on the basis of calculations and simulations presented in Appendix E1 and Figure E1 (*http://radiology.rsnajnls.org/cgi/content/full/2522081550/DC1*).

Ventilation images were acquired by using either a high-spatial-resolution two-dimensional radial protocol or a two-dimensional gradient-recalled echo protocol that exactly matched the lower resolution of the injected ^{129}Xe images. The gradient-recalled echo images were acquired while the animal was continuously ventilated with the 1% xenon mixture flowing directly from the polarizer (25). In this "real-time" mode, as described in the Xenon 129 MR Spectroscopy section, the image was acquired with one k-space view per breath triggered at end expiration (flip angle, 90°; echo time, 6.9 msec; bandwidth, 4 kHz; matrix, 64 × 64; field of view, 6.4 cm). These images thus required approximately 1 minute to obtain and yielded signal-to-noise ratios comparable to those of the injected images. Alternatively, high-spatial-resolution two-dimensional images were acquired during ventilation with fully concentrated hyperpolarized ^{129}Xe prepared by using standard cryogenic accumulation. These images were obtained by using 400 equiangular radial trajectories, acquired in pseudorandom order, by using 10 variable flip-angle radiofrequency pulses (26) per breath (20/0.832; field of view, 4.0 cm) and were reconstructed onto a 128 × 128 Cartesian matrix to yield images with a Nyquist-limited resolution of 312 × 312 μm (17,25).

Figure 2

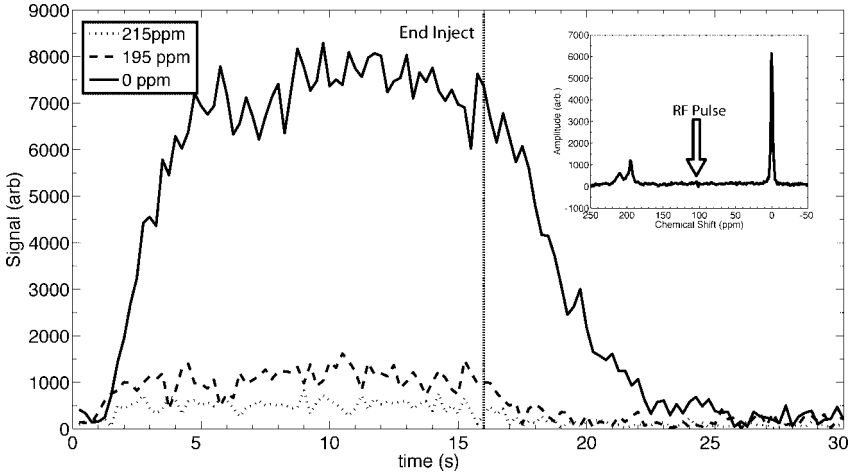

Figure 2: Graph of time course of ^{129}Xe signals during injection of ^{129}Xe-saline mixture in the tail vein depicts the dynamics of the three resonances corresponding to ^{129}Xe in blood (215 ppm), ^{129}Xe in plasma or saline (195 ppm), and gaseous ^{129}Xe in the airspaces (0 ppm). These resonances are shown in the inset spectrum, which was obtained by averaging the signals from 8 to 12 seconds. These spectral dynamics clearly illustrate that the airspace ^{129}Xe peak is dramatically larger (and narrower) than that of the dissolved ^{129}Xe resonances and is the most favorable peak for imaging. The dynamics were probed during a 30-second period at a repetition time of 250 msec, with the injection starting at frame 0 and lasting 16 seconds. *Arb* = arbitrary units, *RF* = radiofrequency.

Results

The temporal dynamics of the three ^{129}Xe resonances, observed by using

Figure 3

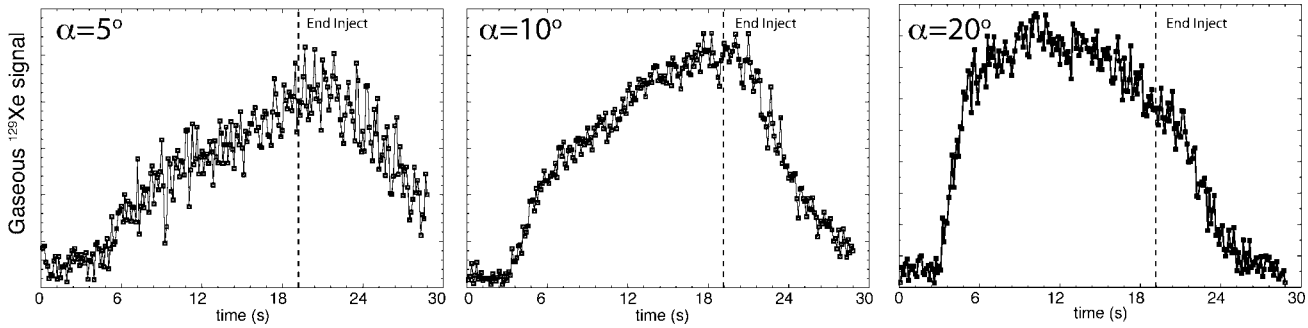

Figure 3: Graphs of dynamics of the gaseous ^{129}Xe signal acquired at various flip angles *(α)* during and after ^{129}Xe-saline injection. Injection started at 0 seconds, simultaneously with data collection, and ended at 19 seconds, as indicated by the dashed line. These data were collected every 125 msec. All experiments showed that signal appeared roughly 3.3 seconds after injection and continued after injection with a decay that was driven by the flip angle.

10° pulses, are depicted in Figure 2, with the inset showing the character of the spectrum at the midpoint of the injection. The spectrum shows three distinct resonances at 215, 195, and 0 ppm corresponding, respectively, to ^{129}Xe in red blood cells; ^{129}Xe in saline, plasma, or tissue; and free ^{129}Xe in the airspaces. The airspace ^{129}Xe signal was considerably larger than that of the dissolved ^{129}Xe because of the relatively low xenon solubility in aqueous environments, thus causing most of the ^{129}Xe to come out of the solution and into the airspaces. A further advantage was that the airspace ^{129}Xe has a longer effective transverse relaxation time (T2*) than dissolved ^{129}Xe because the high diffusivity of ^{129}Xe in the gas phase averages out magnetic field inhomogeneities resulting from the susceptibility gradients at air-tissue interfaces.

Subsequent spectroscopy experiments focusing exclusively on the airspace ^{129}Xe signal were used to optimize the flip angle for imaging and are shown in Figure 3. All signal dynamics studies showed that ^{129}Xe signal first appeared roughly 3.3 seconds ± 0.6 after the start of injection into the tail vein. (For jugular vein injection, gaseous ^{129}Xe signal arrived after a delay of 1.9 seconds ± 0.4, which was consistent with the shorter distance from the jugular injection site to the lungs.)

An example MR image showing results from ^{129}Xe-saline injection and a corresponding high-spatial-resolution ^{129}Xe ventilation MR image are shown in Figure 4. The injected ^{129}Xe image revealed a distinct absence of signal intensity in the region of the right descending mainstem bronchus. This signal void was consistent with expectations, because the major airways are not involved in gas exchange, and thus, no ^{129}Xe would emerge here after injection. The injected image had a signal-to-noise ratio of 25 and a resolution of 1 × 1 mm. This image was generated from a ^{129}Xe volume of approximately 0.5 mL on the basis of a 5-mL injection and 10% xenon Ostwald solubility in the saline and thus represents remarkable efficiency. This rat and all others tolerated the ^{129}Xe-saline injections, which permitted as many as four separate 5-mL injections to be made in a 5-minute period.

Figure 4

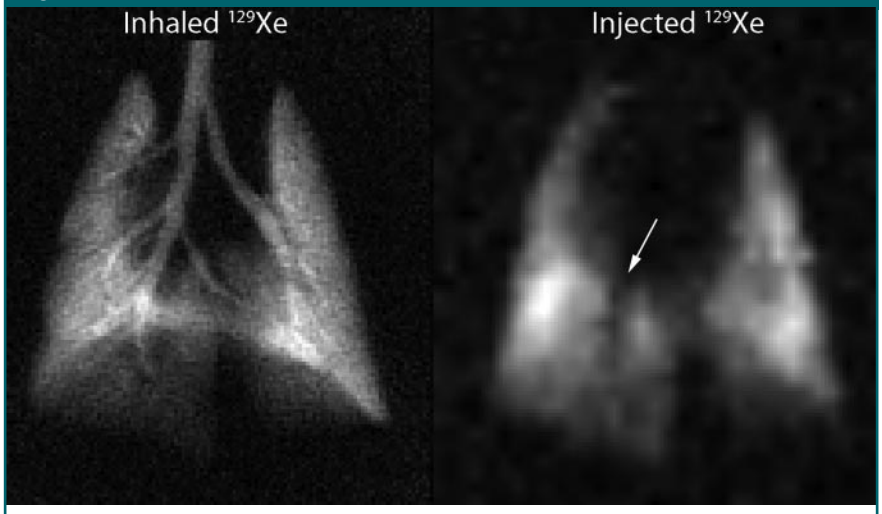

Figure 4: High-spatial-resolution ventilation MR image (left) and MR image acquired with gaseous ^{129}Xe signal emerging in the airspaces after ^{129}Xe-saline injection (right). The injected image shows hypointense region (arrow) in the area of the right descending mainstem bronchus where there is no gas exchange and hence no emerging airspace ^{129}Xe. Both images show gaseous ^{129}Xe; only the delivery method was different.

Figure 5 shows images in a rat that exhibited a matched defect on both the ventilation and the injected ^{129}Xe images. The ventilation image was acquired by using the identical gradient-recalled echo acquisition as for the injected image, but this can cause suppression of the airway

signal due to diffusion-induced attenuation (27). However, this Cartesian sampling requires fewer radiofrequency excitations than radial imaging and therefore is preferable for the injected image. Although this diminishes the airway signal, the image intensity is adequate in the distal lung, where ^{129}Xe diffusion is restricted by the alveolar structure. In the resulting ventilation image, the right cranial lobe contained a hypointense region caused by reduced ventilation that may be associated with regional atelectasis resulting from prolonged mechanical ventilation and is occasionally seen in otherwise healthy control rats in our laboratory. Similar hypointensity was seen on the injected ^{129}Xe image, which indicates that perfusion to this region had been diminished in response to the lack of ventilation.

Figure 6 shows an example of both the sensitivity and the limitations of the ^{129}Xe injection technique. Figure 6 shows images in a smaller rat (200 g), with a normal high-spatial-resolution ventilation image and a baseline injected ^{129}Xe image showing normal perfusion. However, a subsequent injected ^{129}Xe image obtained after the animal had received 10 mL of saline in 2 minutes showed a substantial reduction in emerging ^{129}Xe signal intensity, predominantly in the right lung and at the base of the left lung. This reduction in ^{129}Xe signal intensity likely resulted from hypervolemia (28,29), which causes interstitial thickening of the blood-gas barrier and thereby impairs the diffusion of ^{129}Xe from the vascular to the airspace compartments (17). These images showed that hypervolemia appears to impair gas exchange heterogeneously, which to our knowledge, has not been previously reported. Importantly, the effect was clearly transient, as revealed by the almost full restoration of ^{129}Xe signal intensity on an injected ^{129}Xe image acquired 1 hour later.

Figure 5

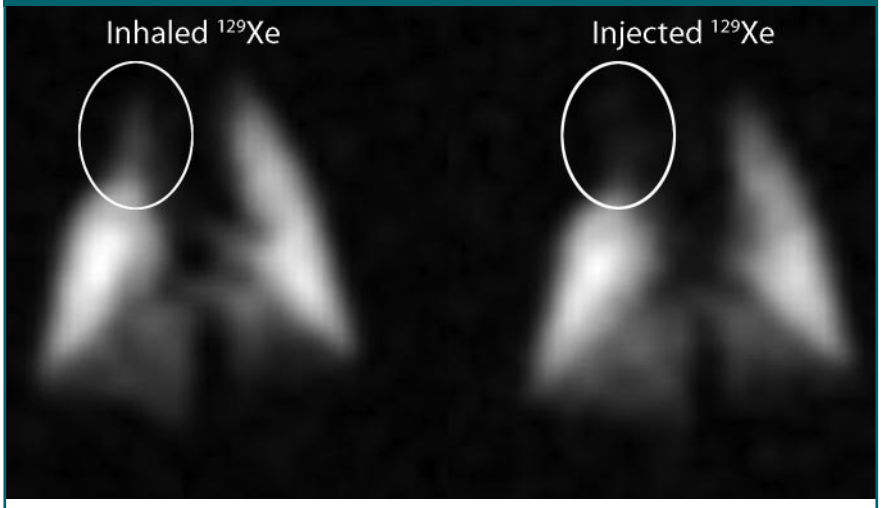

Figure 5: Ventilation (left) and injected (right) ^{129}Xe MR images acquired with an identical sequence and imaging parameters (1 × 1-mm resolution). This particular rat showed reduced ventilation in the right cranial lobe of the lung and matching signal intensity reduction on the injected ^{129}Xe image (circled areas); this likely resulted from reduced perfusion in the same area.

Discussion

We have presented a minimally invasive method based on vascular injection of hyperpolarized ^{129}Xe in saline to generate MR images with contrast driven by pulmonary perfusion and xenon gas exchange. The method, which is proposed as a probe for metabolically important gas

Figure 6

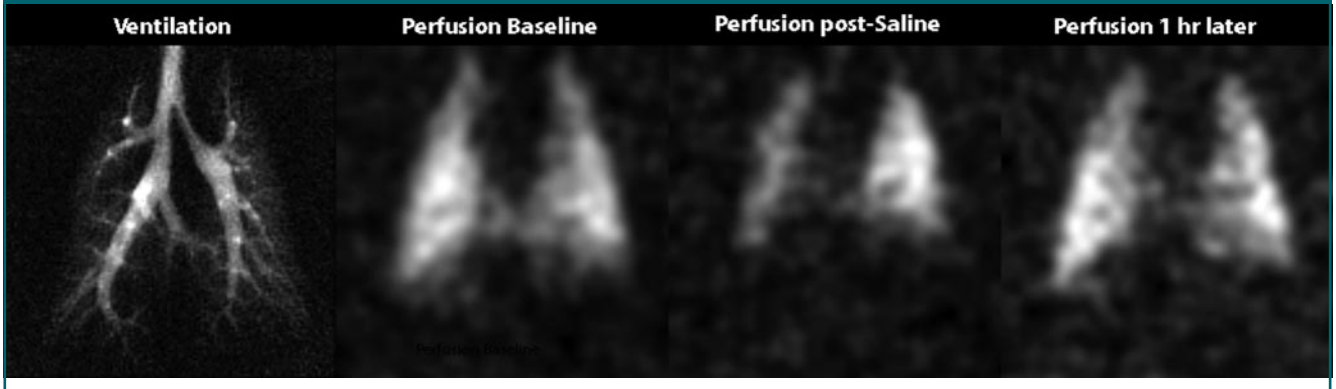

Figure 6: MR images show changes in perfusion and gas exchange caused by saline overloading in 200-g rat. The images are a ventilation image, a baseline injected ^{129}Xe image, and an injected ^{129}Xe image obtained after the rat had received 10 mL of saline in a 2-minute period. This overloading likely caused vascular congestion resulting from hypervolemia and created substantial impairment of xenon exchange in the right lung and the base of the left lung. However, a subsequent perfusion image obtained 1 hour later shows almost complete recovery of perfusion and xenon exchange.

transfer processes, relies on selective detection of only the gaseous ^{129}Xe that emerges in the airspaces of the lung and thus has numerous potential advantages over previous efforts to use hyperpolarized gas MR imaging to indirectly assess pulmonary function. First, because ^{129}Xe was delivered from the vascular side, the resulting images of the lung depended on perfusion directly. Second, image acquisition was based on a simple gradient-echo sequence, where signal intensity showed the underlying transport and exchange of ^{129}Xe directly. Directly imaging ^{129}Xe eliminates the need for postprocessing methods that can complicate image interpretation.

We have thus far resisted referring to the injected ^{129}Xe images as "perfusion images," although the image signal intensity was certainly driven by perfusion. However, as illustrated by the example of saline overload (Fig 6), the technique was also sensitive to impairment of xenon exchange caused by the presence of a barrier to gas diffusion. Although this combination can somewhat complicate the interpretation of the underlying physiology, it also makes the method sensitive to two different aspects of lung physiology. The method would hence help reveal regions of reduced perfusion that could result from an embolism but would also help reveal regions of reduced gas exchange that might be present in interstitial lung diseases or acute lung injury.

This method of using vascular injection of hyperpolarized ^{129}Xe to image perfusion and xenon gas exchange also stands in contrast to more traditional CT- and MR imaging–based approaches to imaging pulmonary perfusion. The latter methods typically rely on injected contrast agents that primarily help visualize the larger blood vessels and capillary blood volume but not gas exchange. By contrast, the injected ^{129}Xe images showed xenon that had traversed the capillary beds and diffused successfully into the airspaces. Because the airspace ^{129}Xe can be distinguished according to its frequency shift from the remaining dissolved ^{129}Xe, there is no question that the arising signal intensity is a direct consequence of pulmonary perfusion and exchange of ^{129}Xe from the dissolved to the gas phase. It stands to reason that such a method should be more sensitive to diseases affecting gas exchange because early stage disease will affect the capillaries before the major vessels.

Translation of the vascular ^{129}Xe delivery method to larger animals or human subjects should be feasible and could be safer than either the injection of traditional gadolinium chelates or iodinated contrast media, which have well-documented adverse effects in certain patient populations (30,31). By contrast, both components of the ^{129}Xe-saline injection are readily cleared by the body.

The present method had two limitations. First, the manual injection of saline may not generate a perfectly stable source of ^{129}Xe signal during imaging. This was illustrated by the declining signal during the 20° spectral acquisitions in Figure 3, even though this flip angle was theoretically predicted to provide a stable signal plateau *(http://radiology.rsnajnls.org/cgi/content/full/2522081550/DC1)*. A more substantial limitation of the method was that increasing image signal-to-noise ratio requires increasing the volume of the ^{129}Xe-saline mixture that is injected. However, we have shown (Fig 6) that large saline volumes can alter xenon exchange, which reflects perturbations in the underlying physiology. While this difficultly can be partially mitigated by using higher-concentration saline solutions to reduce fluid accumulation in the lungs (32), the tolerable saline volume ultimately limits this technique. Thus, an obvious question is whether this vehicle is needed at all. A potentially dramatic improvement would be to infuse the ^{129}Xe directly into the bloodstream at a rate that suitably matches the flow in a particular vessel according to $Q_{Xe} = LQ$, where L is xenon Ostwald solubility and Q is perfusion. Such an infusion may be possible with a catheter designed with a hydrophobic microporous polymer to introduce the ^{129}Xe (33). Because ^{129}Xe is continually cleared through exhalation, the ^{129}Xe infusion could continue as long as necessary to build up the necessary signal to generate high-spatial-resolution three-dimensional images that reflect both perfusion and diffusive transport of ^{129}Xe across the blood-gas barrier.

Acknowledgments: The authors thank Gary Cofer, MS, for help with the MR imaging coil and pulse sequences, Scott Shofer, PhD, MD, for discussions, and Sally Zimney, MED, for assistance in preparing the manuscript. This work was performed at the Duke Center for In Vivo Microscopy, a National Center for Research Resources and National Cancer Institute National Biomedical Technology Resource (P41 RR005959/U24 CA092656).

References

1. Klein JS, Gamsu G, Webb WR, Golden JA, Muller NL. High-resolution CT diagnosis of emphysema in symptomatic patients with normal chest radiographs and isolated low diffusing capacity. Radiology 1992;182:817–821.
2. Beckmann N, Cannet C, Karmouty-Quintana H, et al. Lung MRI for experimental drug research. Eur J Radiol 2007;64:381–396.
3. Croxton TL, Weinmann GG, Senior RM, Wise RA, Crapo JD, Buist AS. Clinical research in chronic obstructive pulmonary disease: needs and opportunities. Am J Respir Crit Care Med 2003;167:1142–1149.
4. Mettler FA. Essentials of nuclear medicine imaging. Philadelphia, Pa: Saunders Elsevier, 2006.
5. Musch G, Layfield JD, Harris RS, et al. Topographical distribution of pulmonary perfusion and ventilation, assessed by PET in supine and prone humans. J Appl Physiol 2002;93:1841–1851.
6. Lam WW, Holdsworth DW, Du LY, Drangova M, McCormack DG, Santyr GE. Micro-CT imaging of rat lung ventilation using continuous image acquisition during xenon gas contrast enhancement. J Appl Physiol 2007;103:1848–1856.
7. Tajik JK, Chon D, Won C, Tran BQ, Hoffman EA. Subsecond multisection CT of regional pulmonary ventilation. Acad Radiol 2002;9:130–146.
8. Won C, Chon D, Tajik J, et al. CT-based assessment of regional pulmonary microvascular blood flow parameters. J Appl Physiol 2003;94:2483–2493.
9. Moller HE, Chen XJ, Saam B, et al. MRI of the lungs using hyperpolarized noble gases. Magn Reson Med 2002;47:1029–1051.
10. Eberle B, Weiler N, Markstaller K, et al. Analysis of intrapulmonary O_2 concentration by MR imaging of inhaled hyperpolarized helium-3. J Appl Physiol 1999;87:2043–2052.
11. Moller HE, Hedlund LW, Chen XJ, et al.

Measurements of hyperpolarized gas properties in the lung: ^{3}He T_1. Magn Reson Med 2001;45:421–430.

12. Patz S, Hersman FW, Muradian I, et al. Hyperpolarized Xe-129 MRI: a viable functional lung imaging modality? Eur J Radiol 2007; 64:335–344.

13. Goodson BM. Nuclear magnetic resonance of laser-polarized noble gases in molecules, materials, and organisms. J Magn Reson 2002;155:157–216.

14. Mansson S, Wolber J, Driehuys B, Wollmer P, Golman K. Characterization of diffusing capacity and perfusion of the rat lung in a lipopolysaccaride disease model using hyperpolarized Xe-129. Magn Reson Med 2003; 50:1170–1179.

15. Ruppert K, Brookeman JR, Hagspiel KD, Mugler JP. Probing lung physiology with xenon polarization transfer contrast (XTC). Magn Reson Med 2000;44:349–357.

16. Ruppert K, Mata JF, Brookeman JR, Hagspiel KD, Mugler JP. Exploring lung function with hyperpolarized Xe-129 nuclear magnetic resonance. Magn Reson Med 2004; 51:676–687.

17. Driehuys B, Cofer GP, Pollaro J, Boslego J, Hedlund LW, Johnson GA. Imaging alveolar capillary gas transfer using hyperpolarized 129Xe MRI. Proc Natl Acad Sci U S A 2006; 103:18278–18283.

18. Driehuys B, Moeller HE, Pollaro J, Hedlund LW. MR imaging of pulmonary perfusion and gas exchange by intravenous injection of hyperpolarized ^{129}Xe [abstr]. In: Proceedings of the Fourteenth Meeting of the International Society for Magnetic Resonance in Medicine. Berkeley, Calif: International Society for Magnetic Resonance in Medicine, 2006; 455.

19. Volgyesi GA, Tremblay LN, Webster P, Zamel N, Slutsky AS. A new ventilator for monitoring lung mechanics in small animals. J Appl Physiol 2000;89:413–421.

20. Driehuys B, Cates GD, Miron E, Sauer K, Walter DK, Happer W. High-volume production of laser-polarized Xe-129. Appl Phys Lett 1996;69:1668–1670.

21. Moller HE, Chawla MS, Chen XJ, et al. Magnetic resonance angiography with hyperpolarized ^{129}Xe dissolved in a lipid emulsion. Magn Reson Med 1999;41:1058–1064.

22. Awad S, Allison SP, Lobo DN. The history of 0.9% saline. Clin Nutr 2008;27:179–188.

23. Bifone A, Song YQ, Seydoux R, et al. NMR of laser-polarized xenon in human blood. Proc Natl Acad Sci U S A 1996;93:12932–12936.

24. Gamblin RL, Carver TR. Polarization and relaxation processes in ^{3}He gas. Phys Rev 1965;138:A946–A960.

25. Driehuys B, Pollaro J, Cofer GP. In vivo MRI using real-time production of hyperpolarized Xe-129. Magn Reson Med 2008;60:14–20.

26. Zhao L, Mulkern R, Tseng CH, et al. Gradient-echo imaging considerations for hyperpolarized Xe-129 MR. J Magn Reson B 1996; 113:179–183.

27. Driehuys B, Walker JK, Pollaro J, et al. 3He MRI in mouse models of asthma. Magn Reson Med 2007;58:893–900.

28. Brown RH, Zerhouni EA, Mitzner W. Visualization of airway-obstruction in-vivo during pulmonary vascular engorgement and edema. J Appl Physiol 1995;78:1070–1078.

29. Staub NC, Nagano H, Pearce ML. Pulmonary edema in dogs, especially sequence of fluid accumulation in lungs. J Appl Physiol 1967; 22:227–240.

30. Broome DR, Girguis MS, Baron PW, Cottrell AC, Kjellin I, Kirk GA. Gadodiamide-associated nephrogenic systemic fibrosis: why radiologists should be concerned. AJR Am J Roentgenol 2007;188:586–592.

31. Morcos SK, Thomsen HS, Webb JAW. Contrast-media-induced nephrotoxicity: a consensus report. Eur Radiol 1999;9:1602–1613.

32. Toung TJ, Nyquist P, Mirski MA. Effect of hypertonic saline concentration on cerebral and visceral organ water in an uninjured rodent model. Crit Care Med 2008;36:256–261.

33. Baumer D, Brunner E, Blumler P, Zanker PP, Spiess HW. NMR spectroscopy of laser-polarized (129)Xe under continuous flow: a method to study aqueous solutions of biomolecules. Angew Chem Int Ed Engl 2006;45: 7282–7284.

Radiology 2009

This is your reprint order form or pro forma invoice

(Please keep a copy of this document for your records.)

Reprint order forms and purchase orders or prepayments must be received 72 hours after receipt of form either by mail or by fax at 410-820-9765. It is the policy of Cadmus Reprints to issue one invoice per order. **Please print clearly**.

Author Name _____
Title of Article _____
Issue of Journal_____ Reprint # _____ Publication Date _____
Number of Pages_____ KB # _____ Symbol Radiology
Color in Article? Yes / No (Please Circle)

Please include the journal name and reprint number or manuscript number on your purchase order or other correspondence.

Order and Shipping Information

Reprint Costs **(Please see page 2 of 2 for reprint costs/fees.)**

_____ Number of reprints ordered $_____
_____ Number of color reprints ordered $_____
_____ Number of covers ordered $_____
Subtotal $_____
Taxes $_____

(*Add appropriate sales tax for Virginia, Maryland, Pennsylvania, and the District of Columbia or Canadian GST to the reprints if your order is to be shipped to these locations*.)

First address included, add $32 for each additional shipping address $_____

TOTAL $_____

Shipping Address **(cannot ship to a P.O. Box) Please Print Clearly**

Name _____
Institution _____
Street _____
City _____ State _____ Zip _____
Country _____
Quantity_____ Fax _____
Phone: Day _____ Evening _____
E-mail Address _____

Additional Shipping Address* **(cannot ship to a P.O. Box)**

Name _____
Institution _____
Street _____
City _____ State _____ Zip _____
Country _____
Quantity _____ Fax _____
Phone: Day _____ Evening _____
E-mail Address _____

** Add $32 for each additional shipping address*

Payment and Credit Card Details

Enclosed: Personal Check _____
Credit Card Payment Details _____

Checks must be paid in U.S. dollars and drawn on a U.S. Bank.

Credit Card: __ VISA __ Am. Exp. __ MasterCard
Card Number _____
Expiration Date_____
Signature: _____

Please send your order form and prepayment made payable to:

Cadmus Reprints
P.O. Box 751903
Charlotte, NC 28275-1903

Note: Do not send express packages to this location, PO Box.

FEIN #:541274108

Invoice or Credit Card Information

Invoice Address **Please Print Clearly**

Please complete Invoice address as it appears on credit card statement

Name _____
Institution _____
Department _____
Street _____
City _____ State _____ Zip _____
Country _____
Phone _____ Fax _____
E-mail Address _____

Cadmus will process credit cards and *Cadmus Journal Services* will appear on the credit card statement.

If you don't mail your order form, you may fax it to 410-820-9765 with your credit card information.

Signature _____ Date _____

Signature is required. By signing this form, the author agrees to accept the responsibility for the payment of reprints and/or all charges described in this document.

RB-1/01/09

Radiology 2009

Black and White Reprint Prices

Domestic (USA only)						
# of Pages	50	100	200	300	400	500
1-4	$239	$260	$285	$303	$323	$340
5-8	$379	$420	$455	$491	$534	$572
9-12	$507	$560	$651	$684	$748	$814
13-16	$627	$698	$784	$868	$954	$1,038
17-20	$755	$845	$947	$1,064	$1,166	$1,272
21-24	$878	$985	$1,115	$1,250	$1,377	$1,518
25-28	$1,003	$1,136	$1,294	$1,446	$1,607	$1,757
29-32	$1,128	$1,281	$1,459	$1,632	$1,819	$2,002
Covers	$149	$164	$219	$275	$335	$393

International (includes Canada and Mexico)						
# of Pages	50	100	200	300	400	500
1-4	$299	$314	$367	$429	$484	$546
5-8	$470	$502	$616	$722	$838	$949
9-12	$637	$687	$852	$1,031	$1,190	$1,369
13-16	$794	$861	$1,088	$1,313	$1,540	$1,765
17-20	$963	$1,051	$1,324	$1,619	$1,892	$2,168
21-24	$1,114	$1,222	$1,560	$1,906	$2,244	$2,588
25-28	$1,287	$1,412	$1,801	$2,198	$2,607	$2,998
29-32	$1,441	$1,586	$2,045	$2,499	$2,959	$3,418
Covers	$211	$224	$324	$444	$558	$672

Color Reprint Prices

Domestic (USA only)						
# of Pages	50	100	200	300	400	500
1-4	$247	$267	$385	$515	$650	$780
5-8	$297	$435	$655	$923	$1194	$1467
9-12	$445	$563	$926	$1,339	$1,748	$2,162
13-16	$587	$710	$1,201	$1,748	$2,297	$2,843
17-20	$738	$858	$1,474	$2,167	$2,846	$3,532
21-24	$888	$1,005	$1,750	$2,575	$3,400	$4,230
25-28	$1,035	$1,164	$2,034	$2,986	$3,957	$4,912
29-32	$1,186	$1,311	$2,302	$3,402	$4,509	$5,612
Covers	$149	$164	$219	$275	$335	$393

International (includes Canada and Mexico))						
# of Pages	50	100	200	300	400	500
1-4	$306	$321	$467	$642	$811	$986
5-8	$387	$517	$816	$1,154	$1,498	$1,844
9-12	$574	$689	$1,157	$1,686	$2,190	$2,717
13-16	$754	$874	$1,506	$2,193	$2,883	$3,570
17-20	$710	$1,063	$1,852	$2,722	$3,572	$4,428
21-24	$1,124	$1,242	$2,195	$3,231	$4,267	$5,300
25-28	$1,320	$1,440	$2,541	$3,738	$4,957	$6,153
29-32	$1,498	$1,616	$2,888	$4,269	$5,649	$7028
Covers	$211	$224	$324	$444	$558	$672

Minimum order is 50 copies. For orders larger than 500 copies, please consult Cadmus Reprints at 800-407-9190.

Reprint Cover

Cover prices are listed above. The cover will include the publication title, article title, and author name in black.

Shipping

Shipping costs are included in the reprint prices. Domestic orders are shipped via FedEx Ground service. Foreign orders are shipped via a proof of delivery air service.

Multiple Shipments

Orders can be shipped to more than one location. Please be aware that it will cost $32 for each additional location.

Delivery

Your order will be shipped within 2 weeks of the journal print date. Allow extra time for delivery.

Tax Due

Residents of Virginia, Maryland, Pennsylvania, and the District of Columbia are required to add the appropriate sales tax to each reprint order. For orders shipped to Canada, please add 7% Canadian GST unless exemption is claimed.

Ordering

Reprint order forms and purchase order or prepayment is required to process your order. Please reference journal name and reprint number or manuscript number on any correspondence. You may use the reverse side of this form as a proforma invoice. Please return your order form and prepayment to:

Cadmus Reprints
P.O. Box 751903
Charlotte, NC 28275-1903

Note: Do not send express packages to this location, PO Box.
FEIN #:541274108

Please direct all inquiries to:

Rose A. Baynard
800-407-9190 (toll free number)
410-819-3966 (direct number)
410-820-9765 (FAX number)
baynardr@cadmus.com (e-mail)

Reprint Order Forms and purchase order or prepayments must be received 72 hours after receipt of form.